Flexural performance of reinforced concrete beams strengthened with fibre reinforced geopolymer concrete under accelerated corrosion

Mohammed Haloob Al-Majidi[1, 2], Andreas P. Lampropoulos[1], Andrew B. Cundy[3], Ourania T. Tsioulou[1], Salam Alrekabi[4]

[1] School of Environment and Technology, University of Brighton, Moulsecoomb, Brighton BN2 4GJ, UK
[2] Department of Civil Engineering, College of Engineering, University of Basrah, Basrah, Iraq
[3] School of Ocean and Earth Science, University of Southampton, Southampton SO14 3ZH, UK.
[4] Department of Civil Engineering, Al-Mustaqbal University College, Babylon, Iraq

Abstract:

The use of additional Reinforced Concrete (RC) layers or jackets is one of the most commonly used techniques for the strengthening of existing structural elements. A crucial parameter for these applications is the durability and the corrosion resistance of the RC layers. However, to date there are not any published studies on the use of novel cementitious materials for the improvement of the durability of the strengthened elements. In this study, a novel strengthening technique is proposed using additional high performance Fibre Reinforced Geopolymer Concrete (FRGC) layers and jackets reinforced with steel bars. The main goal of this technique is the improvement of the structural performance of the existing elements and at the same time the improvement of the durability and corrosion resistance of the strengthening layers. RC beams strengthened with reinforced FRGC layers were examined under standard and accelerated corrosion conditions. Accelerated corrosion tests were performed using the induced current technique followed by flexural tests. The results indicate superior performance for beams strengthened with FRGC and improved performance of the interface between the additional layer and the initial RC beam.

Keywords: Fibre reinforced geopolymer concrete, Reinforced concrete beams, Strengthening, Layers, Accelerated corrosion.

1. INTRODUCTION

Over the last few years interest in the rehabilitation and repair of Reinforced Concrete (RC) structures has increased, as the premature degradation of RC structures exposed to severe environmental conditions and excessive mechanical loading has become an increasingly serious problem. The strengthening of existing structures is of great importance especially in earthquake prone areas, and the efficiency of various techniques for the improvement of their structural performance has been examined in previous studies [1-5]. Many infrastructural elements, such as bridges or tunnels, require, or will require, rehabilitation to overcome the social and economic costs associated with demolition and the subsequent reconstruction of new structures [6]. Some estimates indicate that, globally, in 2010 the expenditure for maintenance and repair work represented about 85% of the total

expenditure in the construction field [7, 8]. The development of long-lasting and effective repair/strengthening methods can greatly reduce these maintenance requirements, improve safety and increase the service life of concrete structures.

RC structures are durable because the steel reinforcement in concrete is prevented from corroding by a thin passive film formed on its surface due to the high alkalinity of the surrounding concrete [9]. However, when the surrounding concrete is not sound or when concrete cover is not sufficient, chloride ions penetrate the cover concrete and reach the steel surface, leading to destruction of the passive film and onset of steel corrosion. In the presence of sufficient oxygen, chloride, and moisture, and if an anodic-cathodic circuit is formed by activation of the steel surface by chloride ions, the steel starts to corrode resulting in decrease of the cross-sectional area of the steel bar and the spalling of the cover concrete, which can lead to deterioration of the RC structural performance [10-12]. Chloride attack is one of the most serious causes of damage to RC structures, because of the ready diffusion of the chloride ion and the rapidity of the deterioration process. Once such deterioration occurs in a reinforced concrete structure, it must be repaired rapidly in order to avoid further degradation and recover lost functionality.

There are numerous research projects and publications focusing on the repair of deteriorated concrete structures. Most of this research uses traditional strengthening techniques based on externally bonded steel plates, reinforced concrete jacketing [13, 14], and use of externally bonded Fibre Reinforced Polymer (FRP), Engineering Cementitious Composite layers with FRP bars, and Textile Reinforced Mortars (TRM) [15-21]. Although all of these techniques can be used with favourable results, there are some limitations. In particular, the use of externally glued FRPs in general leads to a reduced fire resistance and these materials (FRPs and TRM) normally have an increased cost and special expertise is required for the design and application process. On the other hand the use of conventional reinforced concrete jacketing systems require concrete layers and jackets with thicknesses larger than 60–70 mm, as the presence of reinforcing bar requires a minimum concrete cover [6].

Fibre reinforced cementitious composites (FRCC) have been developed and extensively researched over the last two decades [22, 23]. Generally, the addition of fibres to a concrete mix considerably enhances many of the mechanical properties of concrete such as flexural, impact, tensile and abrasion strength, and post cracking behaviour [24, 25]. One of the most promising areas of application of this material is in the strengthening/ repair of concrete structures. Recently, novel techniques using Fibre Reinforced Concrete (FRC) and Ultra High Performance Fibre Reinforced Concrete (UHPFRC) layers or jackets have been proposed to improve the performance of existing structural members [1, 6, 26]. Simultaneously, Fibre Reinforced Geopolymer Concrete (FRGC) is a novel engineering material with the potential to form a substantial element of an environmentally sustainable construction and building products industry [27]. Fibre reinforced geopolymer composites with higher ductility and strain hardening behaviour have been developed in previous studies [25, 27].

Geopolymers are inorganic by-product materials, rich in silicon (Si) and aluminium (Al), that react with alkaline activators to form three dimensional polymeric chains of sialate and poly(sialate) (Si–O–Al–O) [28]. Utilisation of geopolymers as a replacement of conventional concrete can reduce 9% CO_2 [29] and overcome issues related to unregulated disposal of industrial materials by recycling these materials in geopolymer manufacture. Ouellet-Plamondon and Habert (2015) [30] show that only ´one part geopolymers` shows carbon

footprint levels much lower than Portland cement based mixtures. Provis et al. (2015) [31] also emphasized that geopolymers are not intrinsically or fundamentally 'low-CO2' unless designed effectively to achieve such performance, meaning the use of waste based activators, and this was confirmed by Teh et al. (2017) [32]. Besides these environmental benefits, fibre reinforced geopolymer concrete can show significant structural properties improvement over conventional fibre reinforced concrete [25, 27, 28]. Recently, the usage of geopolymer matrix as a repairing layer or as a binding agent to ensure the adhesion between fibre reinforced sheets/ strips and the concrete substrate has been investigated with favourable results [33, 34]. Also, the use of alternative repair mortars based on metakaolin, fly ash and slag, produced by alkali activation technology has been proposed [35]. The development of geopolymeric repair mortars based on low reactive Tunician clay was also presented recently and these mortars were used in addition to metallic grids for the improvement of the flexural strength of beams [35].

The effect of FRGC material on structural behaviour has been rarely studied however and, to date, there are not any published studies on the durability and the efficiency of FRGC layers and jackets for the improvement of the load capacity and ductility of existing RC beams.

The aim of this study is to examine the effectiveness of a newly developed FRGC cured under ambient temperature for strengthening RC beams, and to investigate the resulting improvements in load carrying capacity under standard and accelerated corrosion conditions. The mechanical performance of RC beams strengthened with FRGC was investigated using four-point bending tests. Large scale beams strengthened with additional FRGC layers reinforced with steel bars have been examined. Polyvinyl Alcohol Fibre Reinforced Geopolymer Concrete (PVAFRGC) and Steel Fibre Reinforced Geopolymer Concrete (SFRGC) materials have been used as strengthening materials for the protection of the steel bars of the new layer, and subsequent improvement of the flexural strength of existing beams. Respective specimens strengthened with conventional RC layers have been examined in order to evaluate the effectiveness of (or improvement generated over conventional techniques by) the proposed technique. Accelerated corrosion was undertaken prior to the structural testing of some of the examined specimens using the induced current technique by applying a nominal 300 $\mu A/cm^2$ constant anodic current for approximately 30 days.

2. FRGC MATERIAL PREPARATION AND MECHANICAL PROPERTIES

Fly ash (FA) category S according to BS EN-450 [36], Ground Granulated Blast Furnace Slag (GGBS) and undensified Silica Fume (SF) were used in the current study as geopolymer binders. Silica sand with a maximum particle size of 500 μm was used as an aggregate. The chemical properties of the FA, GGBS and silica sand have been presented in detail in a previous study [28]. Straight steel fibres of 13mm length and Polyvinyl-Alcohol (PVA) fibres of 12 mm length were used in this study (details shown in Table 1). For the alkaline activator, a combination of potassium hydroxide with potassium silicate solution was used.

Table 1. Fibre properties used in this study.

Fibre Type	Length (L_f) [mm]	Diameter (d_f) [mm]	Aspect ratio (L_f/d_f)	Density [g/cm^3]	Tensile strength f_t [MPa]	Elastic modulus E_s [GPa]	Image
Steel	13	0.16	81.25	7.9	2500	200	
PVA	12	0.015	800	1.3	1560± 325	29.5	

A Zyklos high shear mixer (Pan Mixer ZZ 75 HE) was used to manufacture the fibre-reinforced geopolymer composite. Potassium silicate solution with modulus equal to 1.25 was used as an alkaline activator following the procedure described in a previous study [37]. In the examined mix (Table 2), the 93 kg/m^3 of alkaline activator consisted of 66.5 kg/m^3 of Potassium silicate solution and 26.5 kg/m^3 of Potassium hydroxide solution (8M), to form an activator modulus of 1.25.

Geopolymer binder (SF, FA and GGBS) was placed first in the mixer, followed by alkaline liquid, and sand. The liquid phase was prepared in advance by mixing potassium silicate solution with water and Polycarboxylate-based superplasticizer for 5 min prior to mixing with the solid phase. The materials were dry mixed for 5 min and then the liquid phase was added and the mixer run for a further 5 min. After that, steel fibres were gradually added after sieving through an appropriate steel mesh at the top of the mixer, in order to ensure uniform fibre dispersion (and random orientation) in the geopolymer mix. Finally, sand was added to the mixer, and the mixer was run for another 3 min to give a total mixing time of 13 min (Fig. 1). After demoulding, the samples were covered with plastic sheets to prevent moisture loss and cured at room temperature up to the testing date.

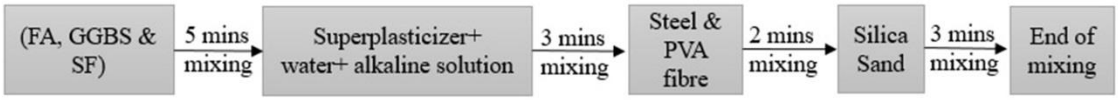

Figure 1. Mixing procedure of FRGC used in the present study.

Standard cube compressive tests (100 mm side) were conducted to evaluate the compressive strength, while for the tensile strength, direct tensile tests of dog bone specimens with cross section (13 mm x 50 mm) were performed, to assess the optimum fibre percentage.

Two geopolymer concrete mixtures with 3% steel and 2% PVA fibre contents were selected for the strengthening of the RC beams since these mixes had a good workability as well as optimum mechanical properties. The selected mix designs and the mechanical properties of both Normal Strength Concrete (NSC) and the PVA and Steel Fibre Reinforced Geopolymer Concretes (PVAFRGC and SFRGC) are presented in Tables 2 and 3.

Table 2. Concretes mix composition. PG = plain geopolymer mix, SFRGC = Steel Fibre Reinforced Geopolymer Concrete, PVAFRGC = PVA Reinforced Geopolymer Concrete, NSC = Normal Strength Concrete.

Material	Mix proportions [Kg/m^3]			
	PG	SFRGC	PVAFRGC	NSC
Fly ash	388	388	388	-
Slag	310	310	310	-
Silica fume	78	78	78	-
Cement	-	-	-	380
Alkaline activator	93	93	93	-
Water	194	194	194	194
Sand	1052	1052	1052	920
Gravel	-	-	-	800
Steel fibre	-	234	-	-
PVA fibre	-	-	26	-

Table 3. Mechanical properties of FRGC.

Material	Compressive strength [MPa]	Tensile strength [MPa]	Elastic modulus [GPa]
SFRGC	70	3.8	25
PVAFRGC	46	3.5	24
NSC	43	3	29

2.1. Shrinkage performance of FRGC

For repair and strengthening applications, the shrinkage of the newly applied concrete is a crucial parameter for the response of the 'composite' elements [1]. In order to evaluate the shrinkage performance of the examined mixes, the drying shrinkage strain of SFRGC and PVAFRGC was measured in accordance with ASTM C 490 [38]. Measurements of the respective Plain Geopolymer (PG) mix were also conducted to evaluate the beneficial effect of the fibres. A digital gauge was used and shrinkage measurements were taken at 1, 3, 5, 7, 14, 21, 28, 56, 90 and 120 days. Drying shrinkage measurements were started 24 hrs after casting. A series of prismatic specimens with cross-sectional dimensions of 75 mm x 75 mm and length of 285 mm were used for the free shrinkage measurements (Fig. 2). The specimens were stored in a room with relative humidity 42% and temperature 20 °C. The average drying shrinkage results of three replicate specimens for all the examined mixtures are presented in Fig. 3.

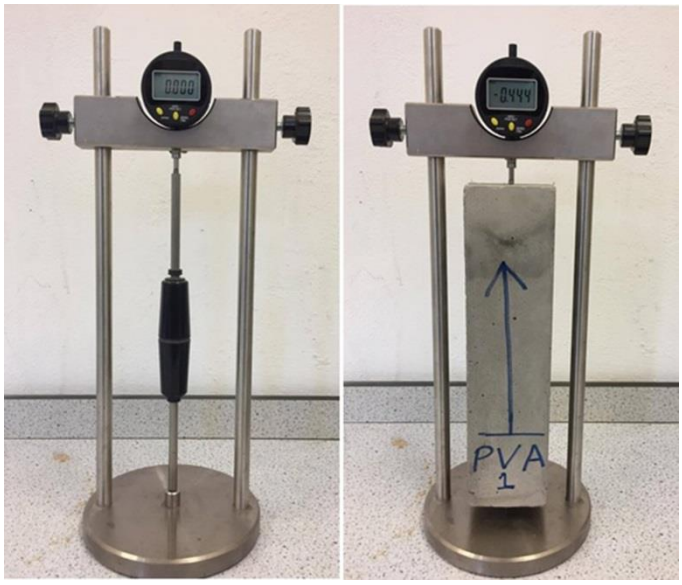

Figure 2. Shrinkage strain measurements setup. Length of specimen on right is 285 mm.

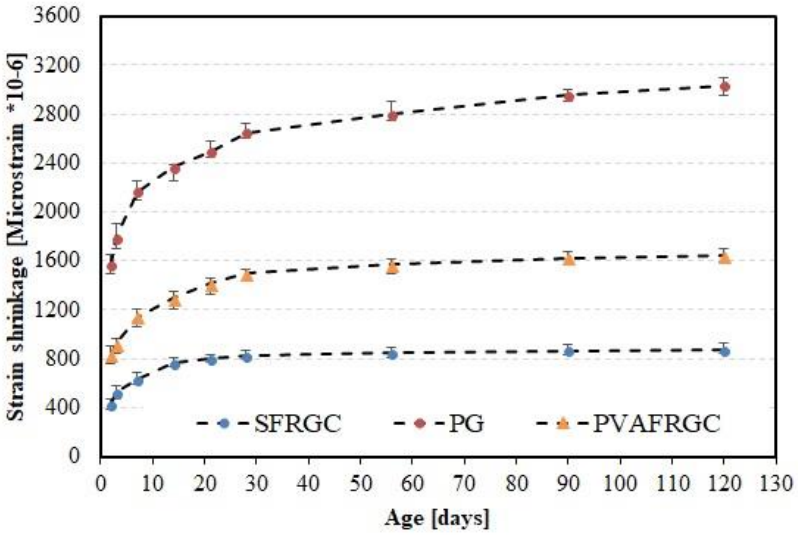

Figure 3. Dry shrinkage results up to 120 days.

Based on the results of Fig. 3 it is evident that the drying shrinkage strain of the PG mortar is very high (around 3000 microstrains) at 120 days, which is in agreement with previous studies [39, 40]. The addition of fibres leads to significant reduction in shrinkage strain values in both cases (i.e. PVAFRGC and SFRGC), especially with the addition of steel fibres (SFRGC). In the case of steel fibres (SFRGC) the shrinkage strain at 120 days was 850 microstrains, while in the case of PVA fibres (PVAFRGC) the respective value was found to be 1600 microstrains. This reduction is attributed to the physical restraint provided by the presence of the fibres in the geopolymer matrix, which is in agreement with previous studies on conventional fibre reinforced concrete [41]. Li *et al.* [41] reported that the reduction of drying shrinkage strain is considerably affected by the volume fraction of the fibres. Atis *et al.* [42] supported this finding and reported that the use of steel fibre restrained movements at the micro level in the case of fly ash and OPC based concrete by bridging and stitching fine shrinkage cracks.

3. EXPERIMENTAL INVESTIGATION OF REINFORCED CONCRETE (RC) BEAMS STRENGTHENED WITH FRGC

3.1. Preparation of the initial (prior to strengthening) RC beams

In total 16 Reinforced Concrete (RC) beams were examined in this study (Table 4). Two beams were used as the 'control' specimens (initial beams), while in all the other specimens different materials were applied in the form of additional layers or jackets for the strengthening of the initial beams (Table 4).

Table 4. Description of the examined specimens.

Specimens description	Specimen designation	Number of specimens
Non-corroded initial RC beams	Ref	2
Non-corroded RC beams strengthened with PVAFRGC layers	PVAFRGC-S	2
Corroded RC beams strengthened with PVAFRGC layers	PVAFRGC-S-corr	2
Non-corroded RC beams strengthened with SFRGC layers	SFRGC-S	2
Corroded RC beams strengthened with SFRGC layers	SFRGC-S-corr	2
Non-corroded RC beams strengthened with NSC layers	NSC-S	2
Corroded RC beams strengthened with NSC layers	NSC-S-corr	2
Non-corroded RC beams strengthened with PVAFRGC 3-side jacket	PVAFRGC-3SJ	2

The geometry and the dimensions of the initial (control) beams are illustrated in Fig. 4.

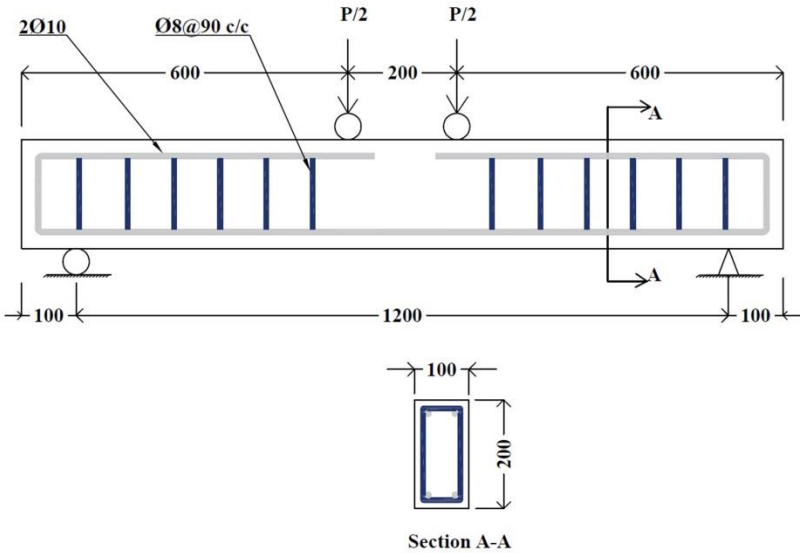

Figure 4. Geometry and reinforcement details of the initial beams (dimensions in mm).

Beams were reinforced in the tensile side with two 10 mm diameter steel bars with yield stress of 530 MPa. Stirrups of 8 mm diameter (Φ8) were used in the shear span at an interval

of 90 mm with a measured yield strength stress value of 350 MPa and spacing 90 mm. Ordinary Portland Cement was used for the casting of the initial beams with coarse aggregate with particle size <10 mm, as well as fine aggregate of 5 mm. During casting, concrete cubes with side dimension 100 mm were sampled and tested for compressive strength, which at the time of structural testing was equal to 32 MPa.

3.2. Strengthening with additional RC layers and investigation of the effect of corrosion

The initial beams (Fig. 4) were cast and left to mature for 3 months [43]. At an age of 90 days, the surfaces of the beams were roughened to a depth of 2–3 mm using an air chipping hammer, representing ‘‘a well-roughened’’ concrete surface texture. These definitions are in agreement with those found in fib Bulletin 55 [44]. Different procedures can be used to evaluate concrete surface texture [45]. The Sand Patch Test according to ASTM E965-96 [46] was used in this study. Strengthening was performed by adding a new concrete layer of 50 mm thickness on the beams’ tensional side (Fig. 5a and 6). Four identical beams were strengthened with an additional layer of each strengthening material (PVAFRGC, SFRGC) while another four identical beams were examined using a conventional strengthening technique whereby an additional layer of Normal Strength Concrete (NSC) was added. In addition, two beams were strengthened by 3-side jacketing using PVAFRGC (Fig. 5b and Fig. 7). In the case of single layer strengthening on the tensile side, the additional layer was reinforced with 2Φ10 steel with a concrete cover of 25 mm (Fig. 5a), while steel bars were not used in the case of 3-side jacketing (Fig. 5b).

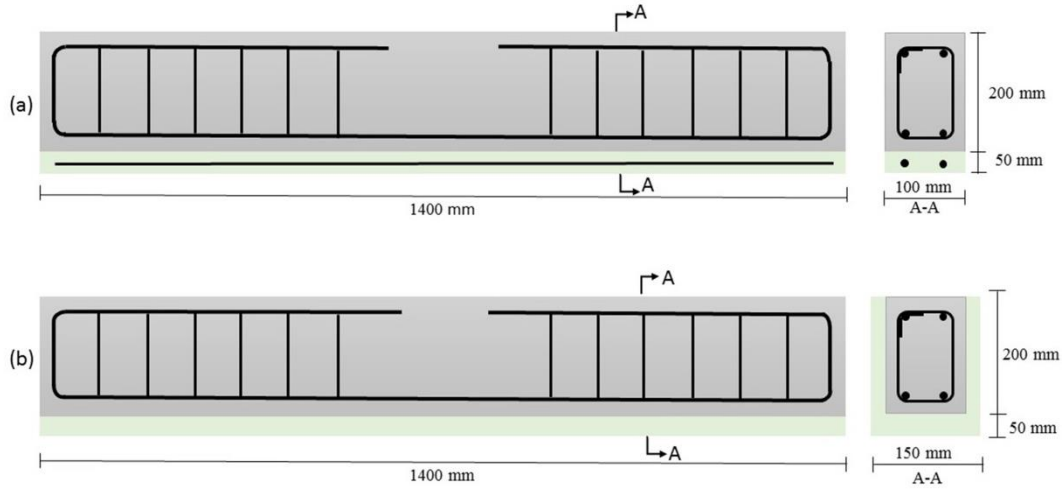

Figure 5. Schematic diagram of strengthening techniques; **a)** Additional layer and **b)** three side jacketing.

(a)

(b)

Figure 6. RC beams **a)** before and **b)** after casting of the strengthening layer.

(a) **(b)**

Figure 7. RC beams **a)** before and **b)** after casting of the three-side jacketing.

All the examined specimens were cured at ambient temperature 21-23ºC and relative humidity 55-60 %, with a plastic sheet being placed on the surface in order to limit water evaporation. After demoulding, the surfaces of the layer or jacket were kept under wet conditions using a water spray for the first 10 days, in order to avoid cracking resulting from differential shrinkage. In some of the examined strengthened specimens, accelerated corrosion by induced current technique was applied 1 month after the casting of the layers. All examined strengthened specimens were tested 2 months after the casting of the layers and 5 months after the casting of the initial beams.

3.2.1. Accelerated corrosion testing by induced current technique

An induced accelerated corrosion test was employed to simulate the corrosion of steel reinforcement in concrete [43]. A schematic of the accelerated corrosion test setup is presented in Fig. 8. Six RC beams were corroded by an accelerated corrosion system, and ten specimens were un-corroded as the reference beams (Table 4). In this corrosion system, RC beams were immersed in a 5% sodium chloride solution. The corrosion process was accelerated by impressing a constant current of 300 mA for 30 days between the reinforcement bar (anode) and a copper mesh (cathode) at the bottom surface of the container connected to the negative terminal of a DC power supply, as shown in Fig. 9.

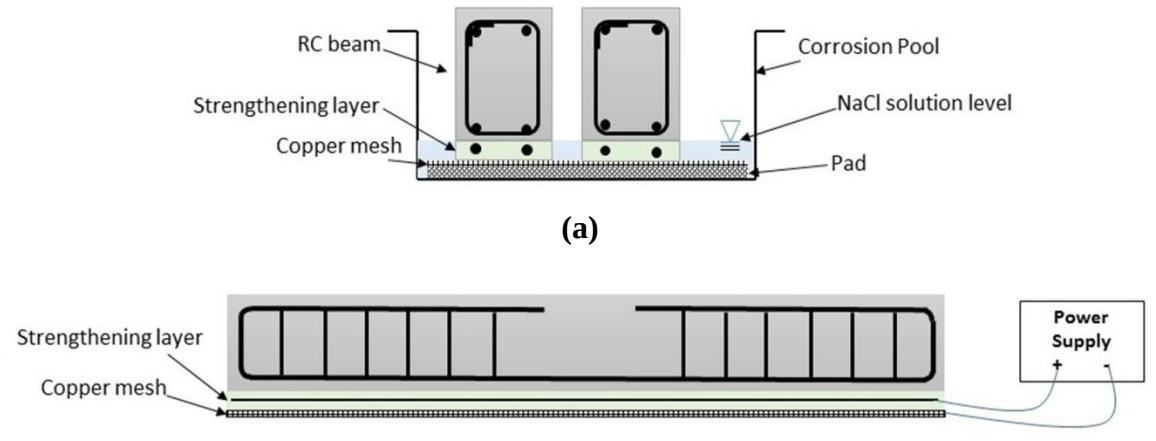

Figure 8. Accelerated corrosion system; **a)** Schematic diagram of corrosion pool and **b)** circuit of accelerated corrosion for strengthening layer.

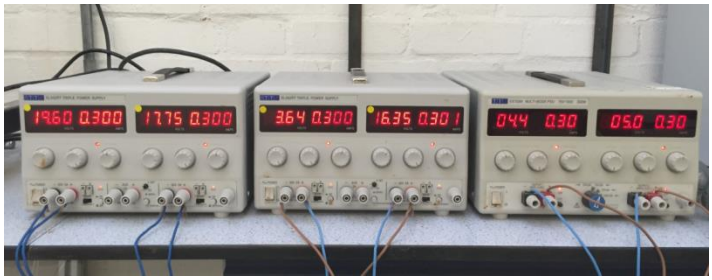

(a)

(b)

Figure 9. Setup for accelerated reinforcement corrosion in RC beam specimens; **a)** Power supply and **b)** specimens under the accelerated corrosion process.

The two steel bars of the additional layer of the strengthened beams were connected to the anodic terminal of the DC power supply (Fig. 8b) in order to evaluate the performance of FRGC layer under severe environmental conditions.

3.2.2. Mechanical test setup

All examined specimens were tested under four-point bending with an effective span equal to 1200 mm (Fig. 10) [43]. A Zwick testing machine was used and the bending tests were conducted under displacement control with a rate of 0.004 mm/s. The displacement of the specimens was measured by Linear Variable Displacement Transducers (LVDT) placed at the centre of the specimen for each side (Fig. 10).

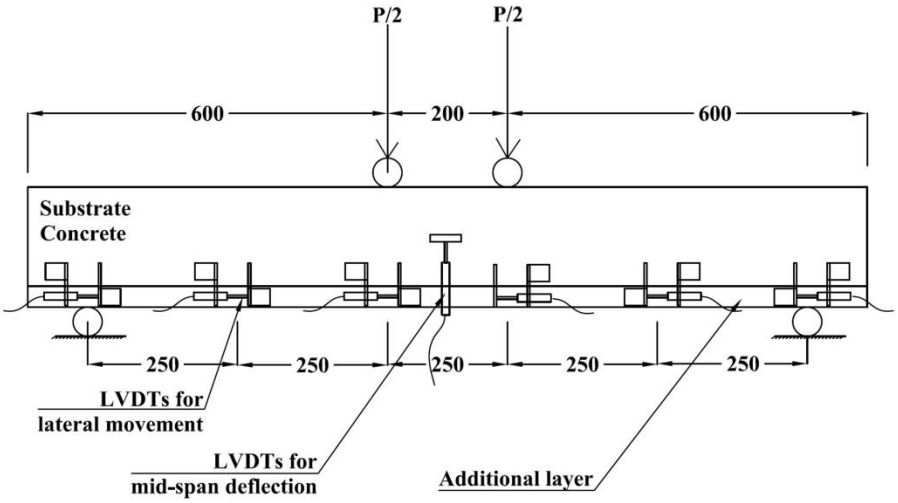

Figure 10. Loading setup of the experimental beams (dimensions in mm).

To record the interface slip at the interface between the strengthening material and the substrate RC beam during the bending tests, six lateral LVDTs were fixed longitudinally to the interface. The LVDTs were attached symmetrically to the beams, three on each side of the load set up (Fig. 11). Fig. 12 presents the typical experimental set up used for the testing of the strengthening beams.

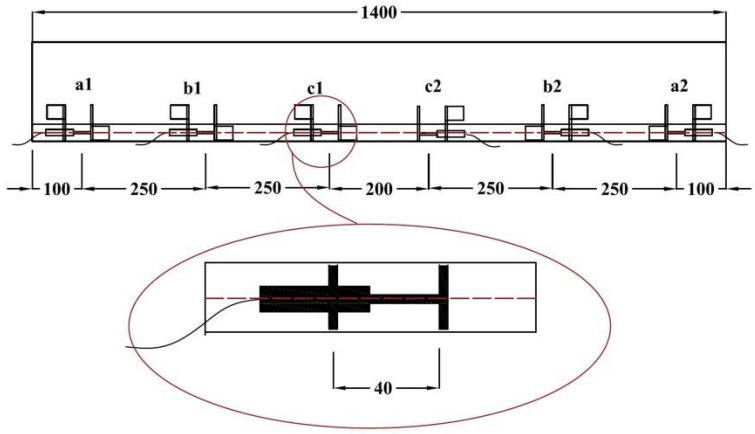

Figure 11. LVDTs used to measure the interface slip (dimensions in mm).

Figure 12. Experimental set up showing the distribution of LVDTs for RC beams.

Each LVDT was glued to the substrate beam and was in contact with a metal angle section that was glued to the strengthening layer. The lateral LVDTs were mounted on the concrete surface at the supports and then at incremental distances of 250 mm towards the centre as shown in Fig. 12.

All readings were continuously collected by data-acquisition systems during the test until the failure of the beam. In addition to the LVDTs, a Digital Image Correlation System (Fig. 13a) was used for the monitoring of part of the interfaces at a distance 250 mm to 500 mm from the end of one side of the beam, at the opposite side to where the LVDTs were placed (Fig. 13b).

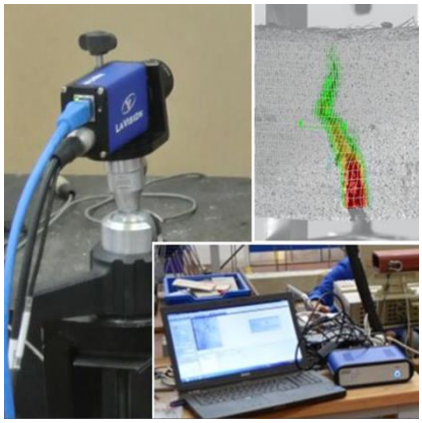

(a)

(b)

Figure 13. a) Digital Image Correlation system and **b)** experimental setup during testing.

4. RESULTS AND DISCUSSION

In this section, experimental test results from beams strengthened by FRGC overlay are presented and discussed. The results include the mode of failure, the load-deflection response and slipping degree at the interface. Steel mass losses due to corrosion processes are also presented and assessed. The results from the corroded beams indicate the effects of corrosion exposure on the flexural response of strengthened RC beams.

4.1. Corrosion damage in strengthened RC beams

The effect of corrosion exposure on the strengthened RC beams was evaluated through visual inspection of crack distribution and mass loss measurements of the steel reinforcement in the additional strengthening layer. Visual inspection indicated that accelerated corrosion exposure of RC beams strengthened with conventional techniques generated rust stains and longitudinal corrosion cracking in the side of the strengthening layer parallel to the corroded steel reinforcing bars. RC beams strengthened with SFRGC showed longitudinal cracks at the bottom and side surface of the additional layer, while RC beams strengthened with PVAFRGC did not show any localized cracks in the additional layer.

Fig. 14 shows the steel reinforcement condition of the repaired beams after corrosion acceleration. The corroded steel reinforcement photos provide examples of the actual corrosion status of reinforcement bars in the additional layer of NSC-S (labelled OPC1 and OPC2 in Fig. 14), PVAFRGC-S (labelled PVA1 and PVA2 in Fig. 14), and SFRGC-S (labelled ST1 and ST2 in Fig. 14).

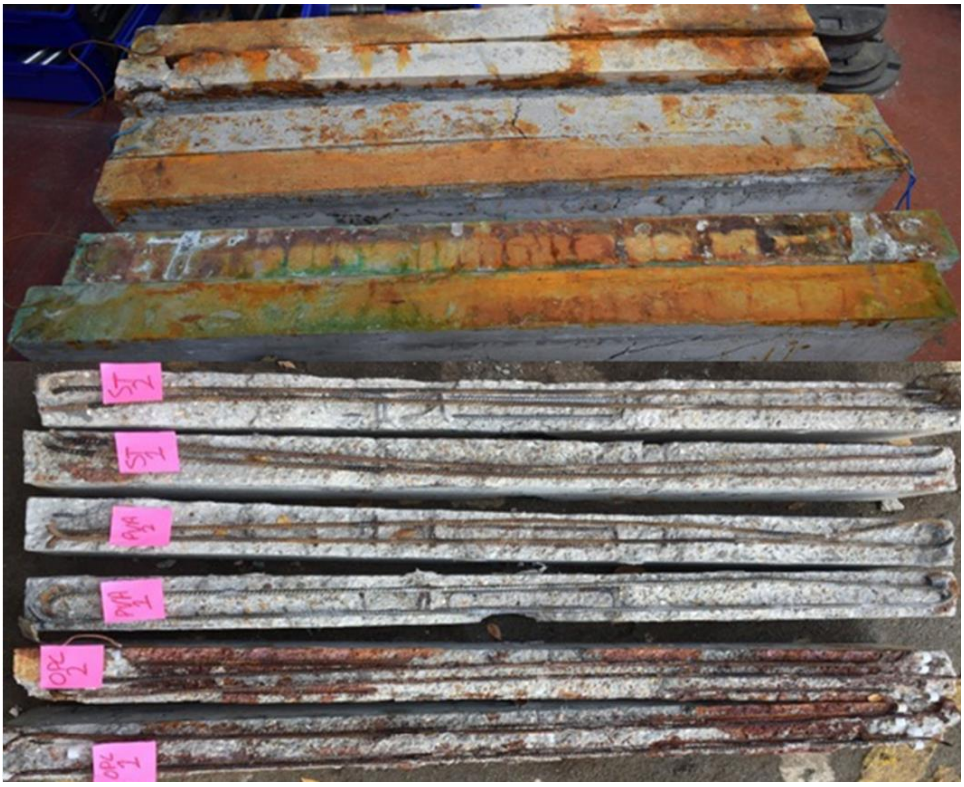

Figure 14. Rebar condition of the strengthened layer following corrosion acceleration.

Corrosion pit formation can be observed on the rebar surface embedded in the NSC layer. In contrast, the reinforcement bars extracted from the additional layers of PVAFRGC and SFRGC had clean surfaces after removal, with less visible corrosion as indicated by a reduction in the weight loss of the rebar.

To quantify differences in the rate of corrosion between the RC beams strengthened with NSC, SFRGC and PVAFRGC, the mass loss measurement is the most reliable method to investigate the degree of corrosion. After demolition of the additional strengthened layer, the reinforcement bars were extracted. To remove the corrosion products from the steel there are various chemical, mechanical and electrolytic techniques described in the ASTM Standard G1-90 [47]. Here, to ensure that the steel bar was free from any adhering corrosion products the rusted steel bars were mechanically cleaned using a stiff metal brush. Average percentages of reinforcement bar mass loss of 11%, 7.5% and 4.5% were recorded after 30 days of accelerated corrosion exposure of RC beams strengthened with NSC, PVAFRGC and SFRGC, respectively. These results indicate that corrosion resistance was increased by using PVAFRGC and SFRGC in retrofitting, rather than conventional reinforced concrete, with the greatest mass loss reduction observed when using SFRGC. The reduction in corrosion damage observed for PVAFRGC and SFRGC strengthened specimens is due to the decreased permeability for water and chloride ion ingress.

4.2. Mode of Failure and crack patterns

The failure modes of the strengthened RC beams with additional layers of NSC, PVARGC, and SFRGC are shown in Fig. 15.

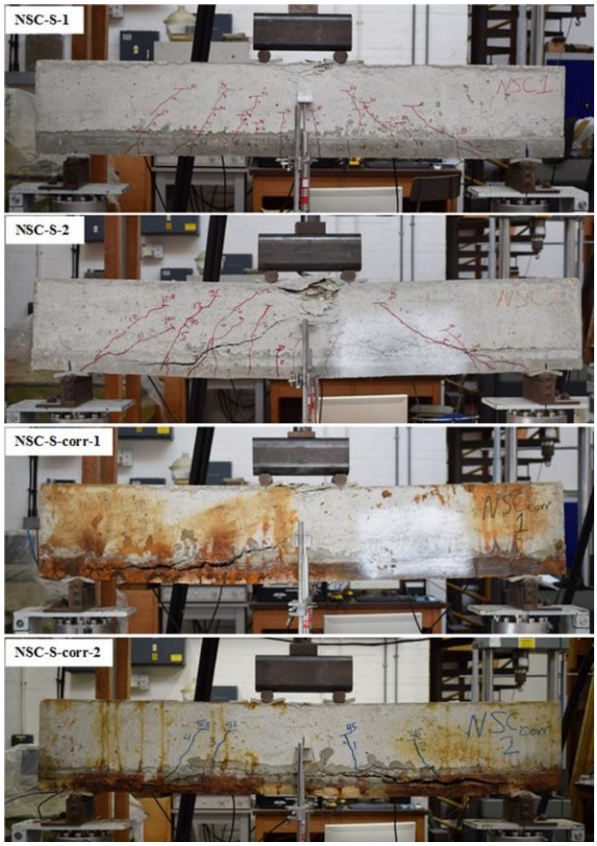

(a)

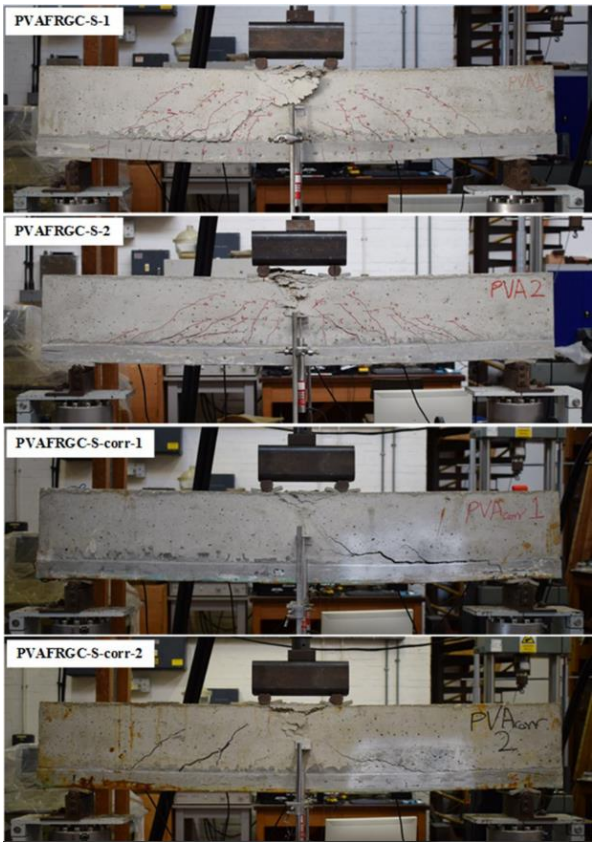

(b)

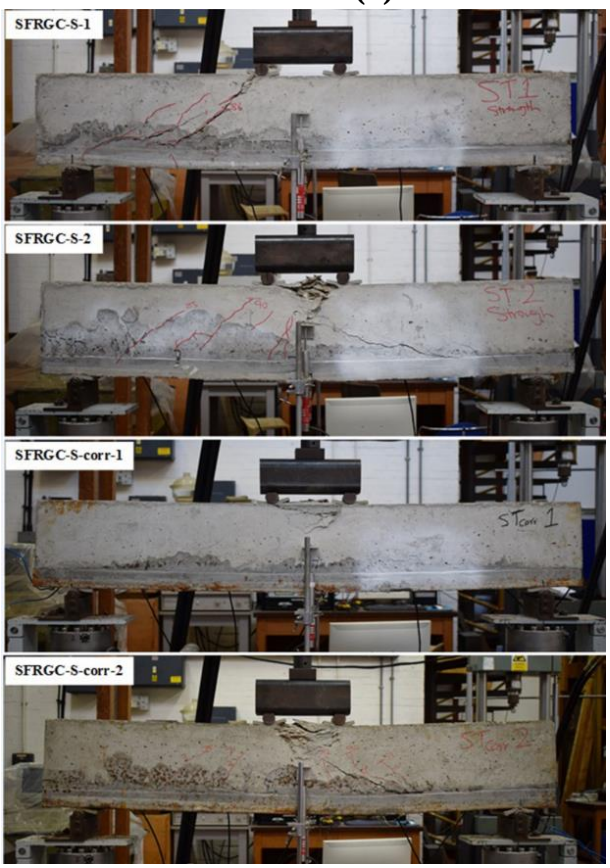

(c)

Figure 15. Mode of failure of RC beam strengthened **a)** with NSC, **b)** with PVAFRGC, and **c)** with SFRGC.

The RC beams strengthened by an additional reinforced normal strength concrete layer failed by concrete crushing at the compressive side, followed by shear cracking. For the corroded specimens strengthened by NSC, accelerated corrosion damage and large longitudinal cracks caused spalling of the concrete cover. The corroded beams under loading failed by shear cracking followed by peeling off of the concrete cover layer i.e. separation of the concrete cover from the additional layer (Fig. 15a). The RC beams strengthened by the additional PVAFRGC layer failed by concrete crushing at the compression side followed by de-bonding at the interface between the PVAFRGC layer and the substrate concrete. Cracks were widely distributed along the specimens' length with significant bendable performance. Corrosion exposure of RC beams strengthened by PVAFRGC did not change the failure mode (Fig. 15b). For the beams strengthened with the SFRGC layer, the failure for the first specimens occurred by shear failure under one of the point loads and the second beam failed by crushing of concrete at the compression side followed by shearing cracking. The corroded specimens strengthened by SFRGC showed similar cracking patterns under flexural loading (Fig. 15c).

4.3. Loading capacity of strengthened RC beams

The geopolymer-layer strengthened RC beam results were compared with loading capacity results from the RC beams strengthened with NSC to evaluate the structural performance of the PVAFRGC and SFRGC strengthening system. Loads at two points (at the first crack load and at the peak load) are considered for the evaluation of the experimental results. A comparison of the load deflection curves of the non-corroded and corroded strengthened beams with single strengthening/repair layers is presented in Fig. 16, while in Fig. 17 load deflection results for the non-corroded RC beam strengthened with 3 side jacketing are presented.

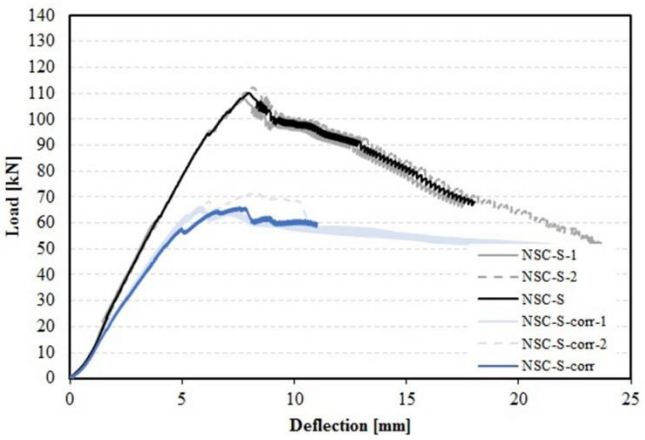

(a)

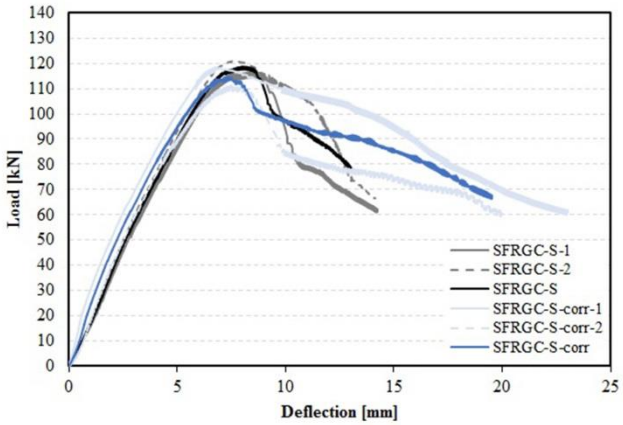

(b)

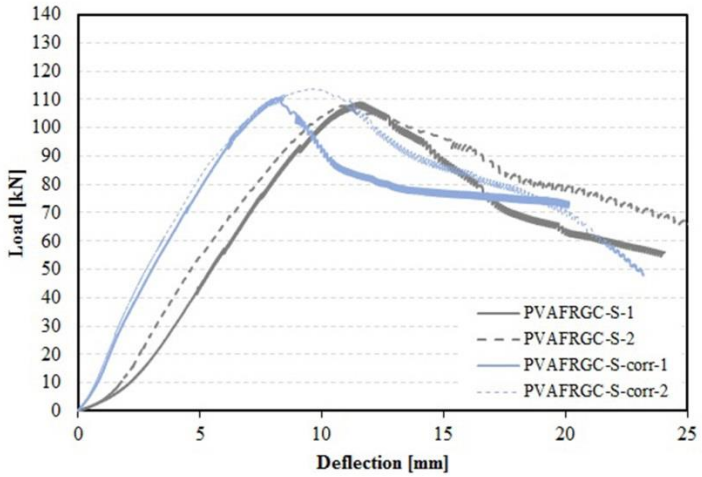

(c)

Figure 16. Load against deflection curve comparisons between corroded and non-corroded strengthened RC beams with **a)** NSC layer, **b)** SFRGC layer and **c)** PVAFRGC layer. Curves labelled with suffix "corr" are those for corroded specimens.

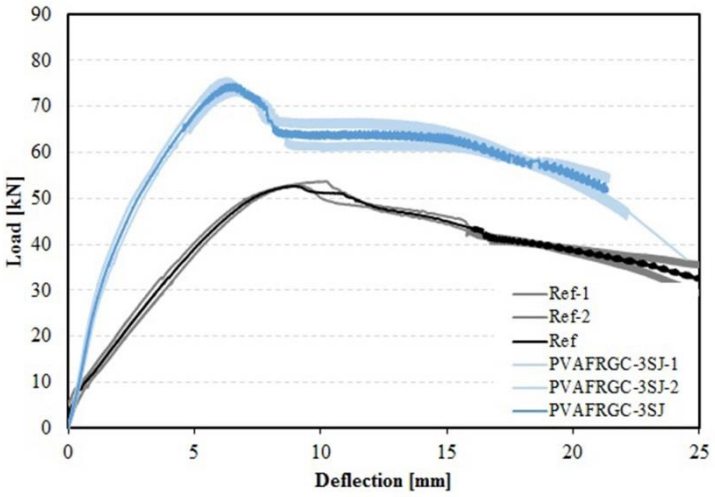

Figure 17. Load against deflection curve comparisons between the initial RC beams (labelled with prefix "Ref"), and RC beams strengthened with 3 sides jacketing using PVAFRGC.

Comparisons of the experimental results for the point of first cracking and the peak load are presented in Tables 5 and 6 for the non-corroded and for the corroded specimens, respectively.

Table 5. Test results of the non-corroded strengthened RC beams at the first cracking load and at the peak load.

Specimen ID	First crack load				Peak load			
	Load [kN]	Increase w.r.t. reference beam [%]	Increase w.r.t. NSC-S specimens [%]	Deflection [mm]	Load [kN]	Increase w.r.t. reference beam [%]	Increase w.r.t. NSC-S specimens [%]	Deflection [mm]
Ref	9.2			0.73	53			9.9
NSC-S	23.5			1.75	109.6			8.05
PVAFRGC-S-1	29.7	223	27	3.9	109.0	106	-1	11.56
PVAFRGC-S-2	30.7	233	31	3.13	104.7	98	-4	11.10
SFRGC-S-1	35.8	289	53	2.02	116.5	120	6	8.75
SFRGC-S-2	38.7	321	65	1.95	120.8	128	10	7.90
PVAFRGC-3SJ-1	25.0	172	7	0.90	76.3	44	-30	6.30
PVAFRGC-3SJ-2	26.6	189	13	1.15	73.4	39	-33	7.16

Table 6. Test results of the corroded strengthened RC beams at the first cracking load and at the peak load.

Specimen ID	First crack load			Peak load		
	Load [kN]	Increase w.r.t. NSC specimens [%]	Deflection [mm]	Load [kN]	Increase w.r.t. NSC specimens [%]	Deflection [mm]
NSC-S-corr	20.2		1.7	68.7		7
PVAFRGC-S-corr-1	26.8	33	1.63	110.5	61	8.14
PVAFRGC-S-corr-2	28.6	41	1.6	113.5	65	9.62
SFRGC-S-corr-1	24.5	21	0.75	118.5	72	6.79
SFRGC-S-corr-2	22.8	13	1.19	111.4	62	7.49

At the first cracking point, strength increases of 155%, 228% and 305% were observed by the addition of NSC, PVAFRGC and SFRGC layers respectively. The average peak load values increased by 107%, 102% and 124% for NSC-S, PVAFRGC-S and SFRGC-S specimens compared to the control beams (Table 5). Overall, the behaviour of all the examined beams strengthened with reinforced layers without corrosion was broadly similar, with optimum structural performance observed in beams strengthened with SFRGC. This is attributed to the presence of 2Φ10 mm reinforcement bar in all of the additional layers, which contributed additional flexural capacity to each RC beam. However, the deflection at the peak load of PVAFRGC-S specimens was around 11.2 mm, higher than NSC-S and SFRGC specimens at 8.32 mm and 8.05 mm, respectively.

For the corrosion damaged specimens, the average first crack load of the RC beam strengthened with NSC was considerably reduced (by approximately 16%), while the average peak load value was reduced by 37.5% compared to the non-corroded specimens (Fig. 16a). In the case of PVAFRGC-S-corr specimens, accelerated corrosion did not have a significant detrimental effect, with average peak load values found to be quite close and even slightly higher (5%) compared to the non-corroded PVAFRGC-S specimens (Fig. 16b). The ultimate failure load values of corroded and non-corroded RC beams strengthened with SFRCG layers were quite similar, at 118.7 kN and 115 kN, respectively (Fig. 16c). Compared to the NSC-S-corr, the first crack load values increased by 37% and 17% for PVAFRGC-S-corr and SFRGC-S-corr specimens, respectively, on average. The peak loads of the PVAFRGC-S-corr and SFRGC-S-corr specimens were higher than the NSC-S-corr specimens by 63% and 67.3%, respectively. The strengthened RC beams with non-reinforced PVAFRGC jacketing improved the load values by 172% and 189% at the first crack load, while the peak load was increased by 44% and 39%, respectively, compared to the reference RC beam (Fig. 17).

A comparison between RC beams strengthened with NSC, PVAFRGC and SFRGC revealed that an increment in the compressive strength of the strengthening layer from 43 MPa to 70 MPa had negligible influence on the flexural capacity of the strengthened RC beams. However, RC beams strengthened with SFRGC and PVAFRGC showed significantly enhanced corrosion resistance. Accumulated corrosion products around the reinforcement bar increased the pressure on the surrounding concrete in all directions. At the early stage of corrosion, internal pressure generally strengthened the bond between the reinforcing bar and the surrounding concrete. These positive effects of slight corrosion are observed on the load-deflection curves of the RC beams strengthened with SFRGC and PVAFRGC after 7.5% and 4.5% mass loss, respectively. The overall enhancement in corrosion resistance of both types of FRGC layering can be attributed to the fact that when the FRGC overlay is used, the crack widths generated by the corrosion products surrounding the reinforcement bars are reduced. Cracking, particularly large cracks, allow the conductive chloride solution to come into direct contact with the steel surface, consequently providing a direct current path between the steel reinforcement bars and the electrodes and resulting in a reduction in electrical resistance following cracking in the cementitious material around the steel bar [48, 49].

4.4. Interface slip measurement of strengthened specimens

Fig. 18, Fig. 19 and Fig. 20, illustrate the relationship between load and slip measurements in the RC beams strengthened with NSC, PVAFRGC and SFRGC, respectively. The geometry of the strengthened overlay was symmetrical and the preparation of the interface was the same along the whole of its length. Thus, the slip measurements against the load are controlled by the differential crack development at the interface with different overlay materials under flexural loading.

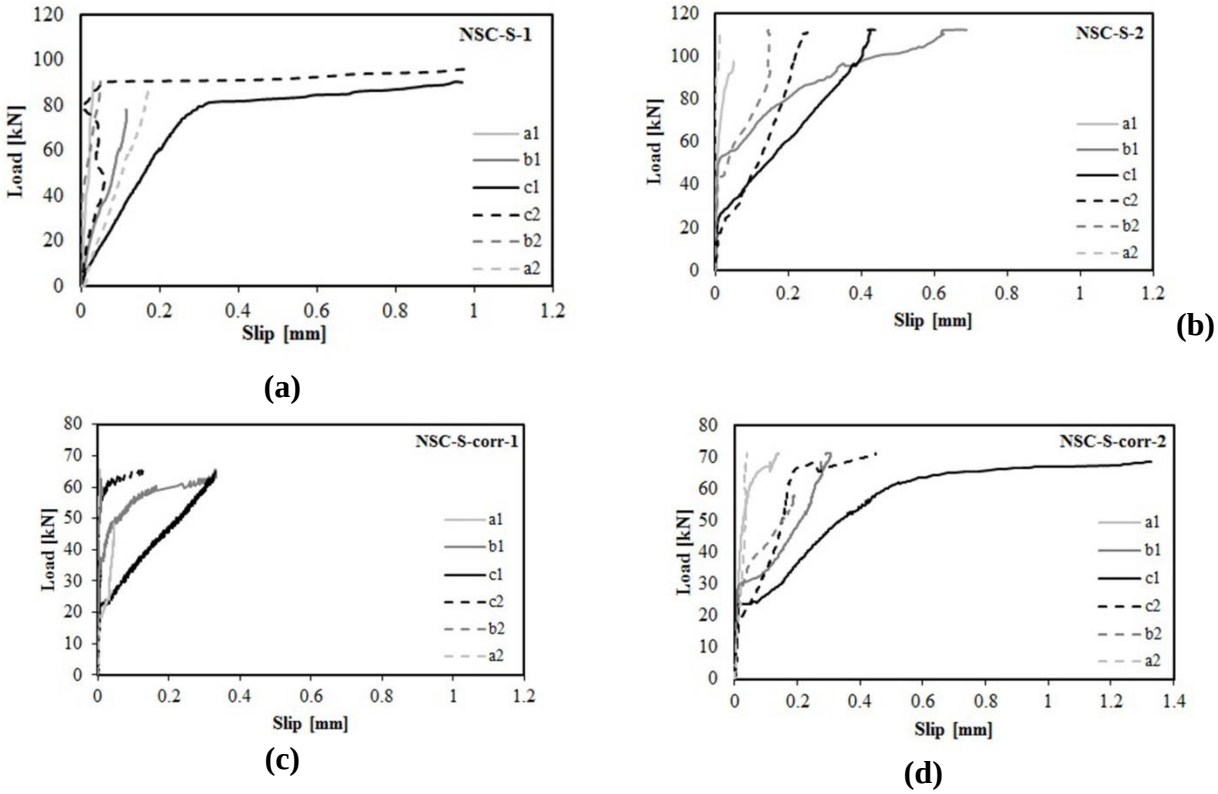

Figure 18. a-d) Load versus slipping relationship of RC beams strengthened with NSC overlays. Graphs labelled with suffix "corr" show results for specimens which have undergone accelerated corrosion.

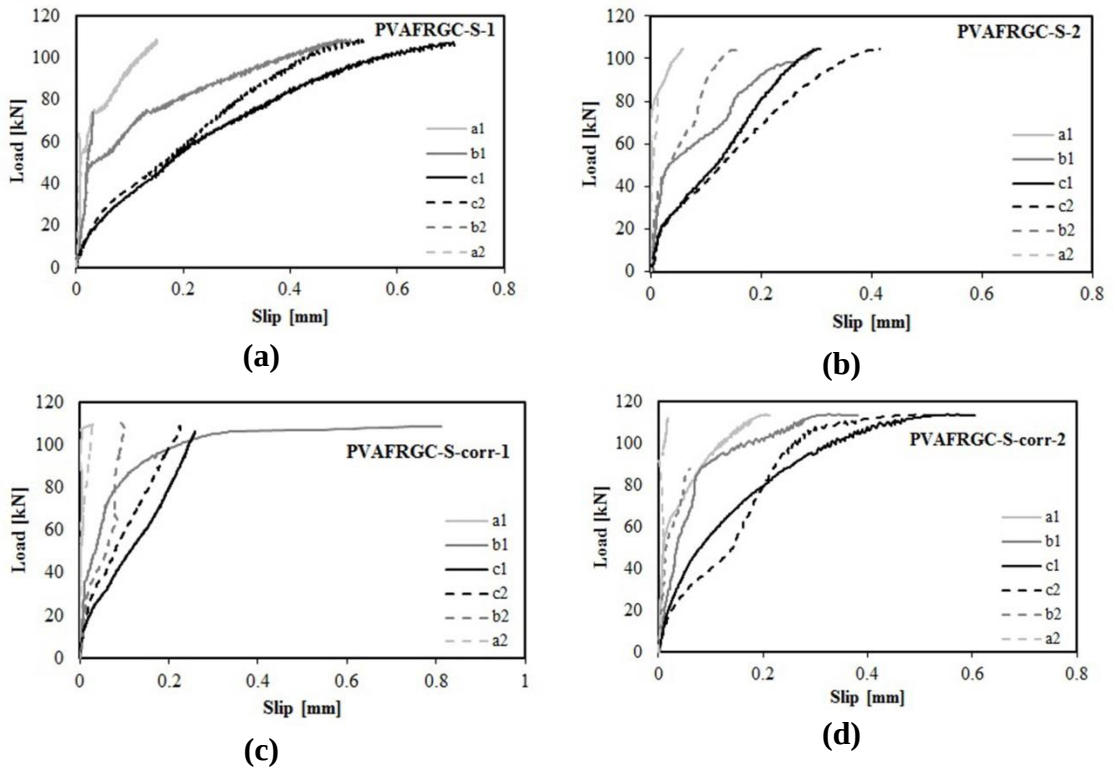

Figure 19. a-d) Load versus slipping relationship of RC beams strengthened with PVAFRGC overlays. Graphs labelled with suffix "corr" show results for specimens which have undergone accelerated corrosion.

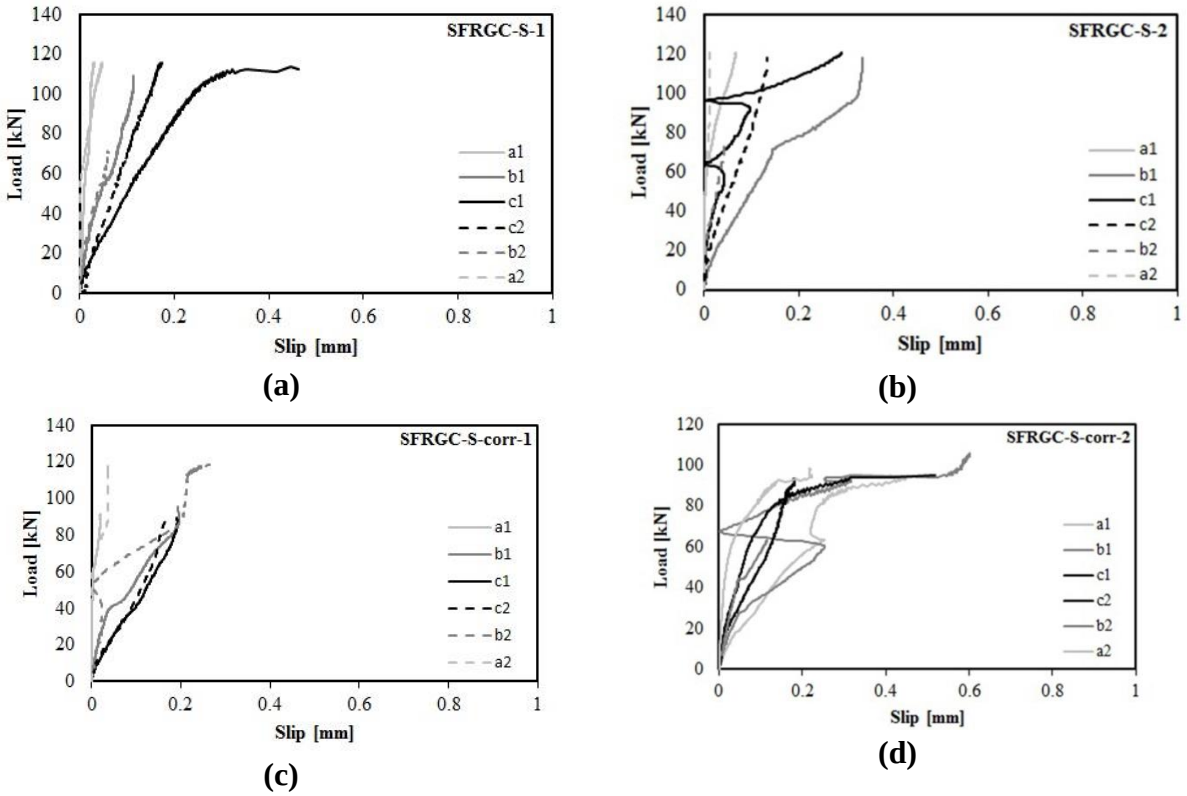

Figure 20. a-d) Load versus slipping relationship of RC beams strengthened with SFRGC overlays. Graphs labelled with suffix "corr" show results for specimens which have undergone accelerated corrosion.

From Fig. 18, Fig. 19 and Fig. 20, the interface slip values are summarized in Table 7, which shows the maximum load (P_{max}) and the maximum slip (s_{max}) alongside the respective loads at interface slip values of 0.2 mm ($P_{s=0.2\ mm}$), 0.8mm ($P_{s=0.8\ mm}$) and 1.5 mm ($P_{s=1.5\ mm}$). These are the ultimate accepted slip values for immediate occupancy, life safety and collapse prohibition behaviour levels respectively according to GRECO [50, 51].

Table 7. Maximum load and slip values for the strengthened RC beams.

Specimen	P_{max} [kN]	S_{max} [mm]	$P_{(s=0.2\ mm)}$ [kN]	$P_{(s=0.8\ mm)}$ [kN]	$P_{(s=1.5mm)}$ [kN]
NSC-S-1	106.8	1	60.0	87.0	--
NSC-S-2	112.2	0.69	60.7	--	--
NSC-S-corr-1	66.1	0.32	45.7	--	--
NSC-S-corr-2	71.3	1.33	36.8	65.7	--
PVAFRGC-S-1	109.0	0.70	57.9	109.0	--
PVAFRGC-S-2	104.7	0.41	67.4	--	--
PVAFRGC-S-corr-1	110.5	0.82	80.1	80.6	--
PVAFRGC-S-corr-2	113.6	0.6	79.3	--	--
SFRGC-S-1	116.5	0.46	87.8	--	--
SFRGC-S-2	120.8	0.34	78.2	--	--
SFRGC-S-corr-1	118.5	0.26	82.0	--	--
SFRGC-S-corr-2	111.4	0.60	50.0	--	--

According to slip measurements of the RC beams strengthened with NSC overlay (Fig. 18 and Table 7), the maximum interface slip varied depending on the failure mode and crack propagation along the RC beam substrate and the overlay material. Overall the specimens with the Fibre Reinforced Geopolymer Layers (PVAFRGC and SFRGC) show relatively small values of interface slip (0.34-0.82 mm). Therefore it can be concluded that the obtained slips are in general acceptable for life safety levels for which a limit of 0.8 mm has been specified by GRECO [50, 51]. The highest slip values were observed for the specimens strengthened with Normal Concrete with and without corrosion where maximum slip values of 1.33 mm (NSC-S-corr-2) and 1 mm (NSC-S-1) were recorded and therefore they are complying with the limit for collapse prohibition level for which the maximum slip value is 1.5 mm [50, 51].

Shear strain values were also obtained using a Digital Image Correlation System and indicative results for PVAFRGC overlay are presented in Fig. 21a, Fig. 21b, and Fig. 21c for mid-span deflection values equal to 10 mm, 12 mm and 20 mm respectively.

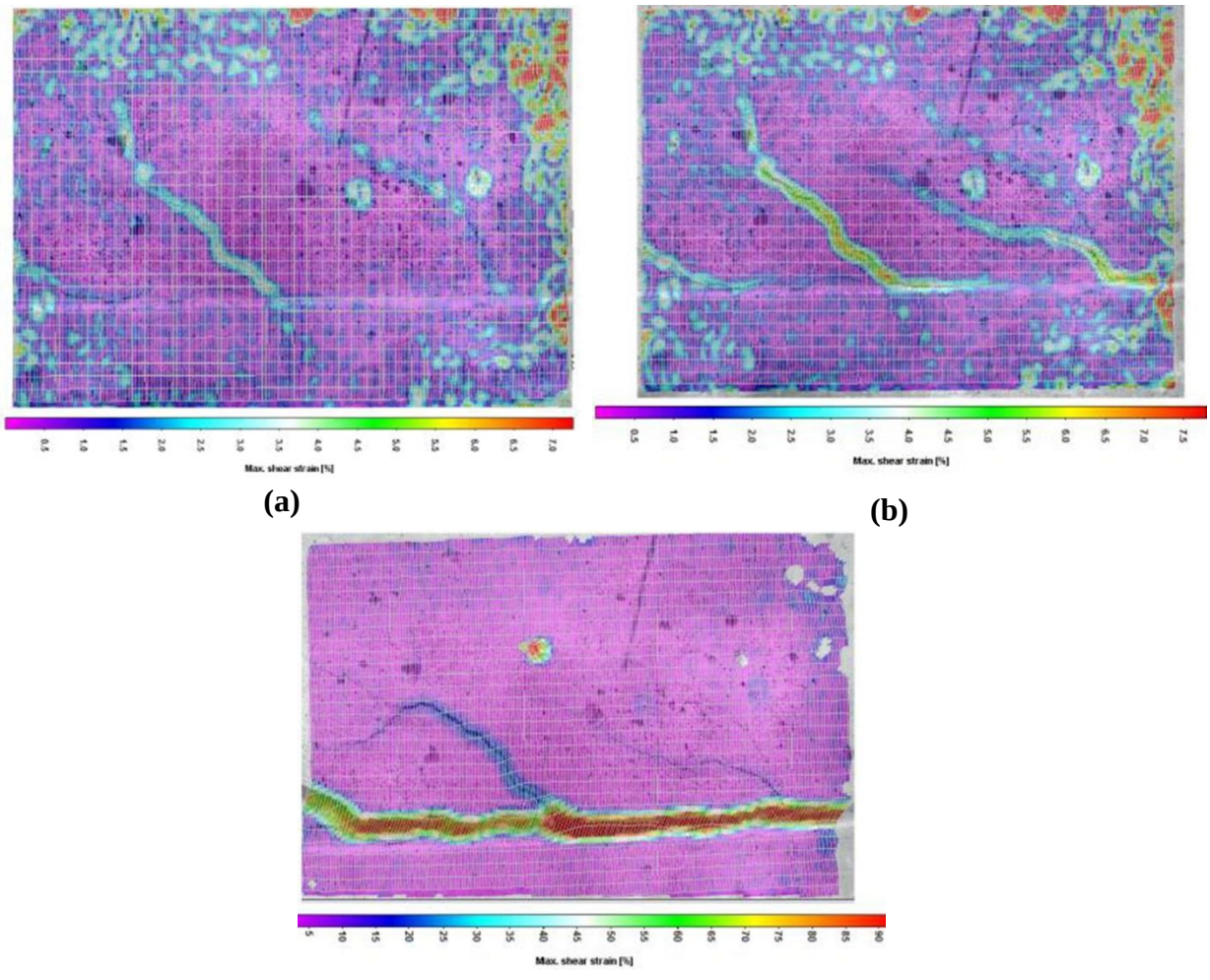

Figure 21. Digital Image Correlation results for shear strain values at approximate mid-span deflection values **a)** 10mm, **b)** 12mm, and **c)** 20mm, for PVAFRGC overlay.

The results show that for mid-span deflection equal to 10 mm which corresponds to a load value near the maximum load, there is not any shear strain concentration at the interface which is in agreement with the relatively low slip measurements of Fig. 19. Then, and after the peak load, there are some shear strain concentrations at the interface (Fig. 21b and c) which are attributed to the crack propagation of the shear cracks from the initial beam to the PVAFRGC overlay.

The interface slip measurements along the beam length for RC beams strengthened with NSC, PVAFRGC and SFRGC respectively are presented in Fig. 22, 23 and 24.

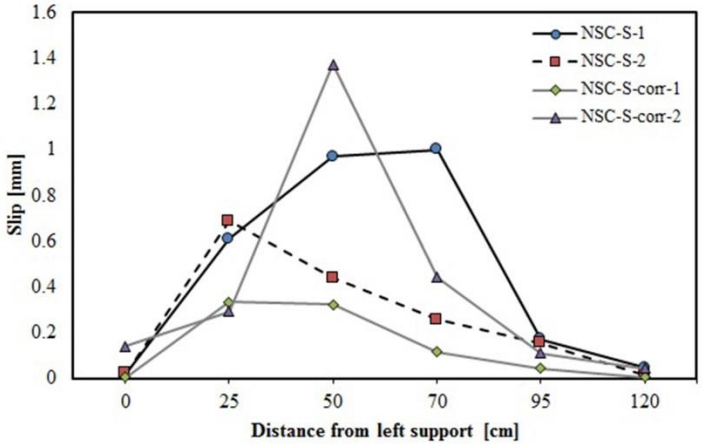

Figure 22. Interface slip measurements at peak load for strengthened RC beams with NSC overlay.

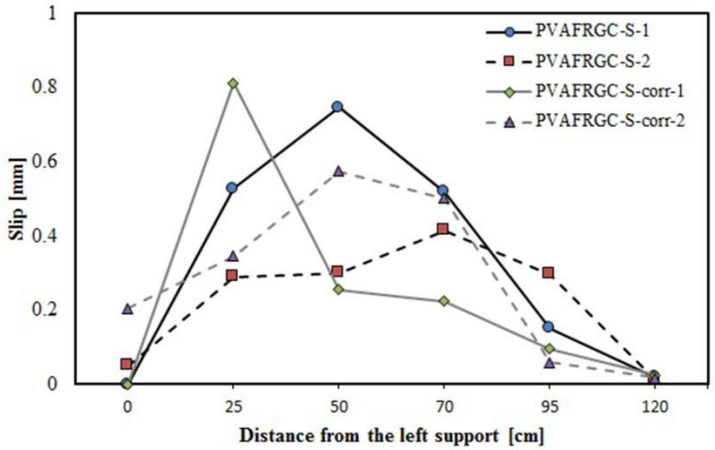

Figure 23. Interface slip measurements at peak load for strengthened RC beams with PVAFRGC overlay.

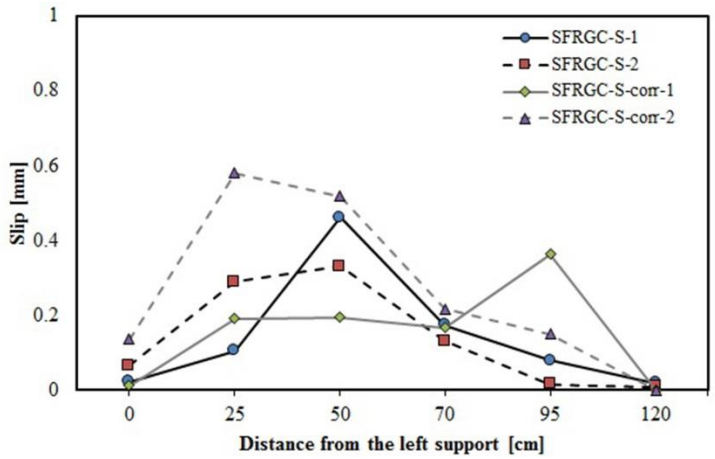

Figure 24. Interface slip measurements at peak load for strengthened RC beams with SFRGC overlay.

By comparing Fig. 22, 23 and 24, it is obvious that overall lower maximum slip values were observed in the case of specimens strengthened with reinforced PVAFRGC and SFRGC layers, compared to the respective results of specimens strengthened with reinforced NSC layers. This confirms the improved interface conditions of the specimens strengthened with PVAFRGC and SFRGC layers. The interface slip measurements at the supports were found to have the smallest values, which increased as bending cracks began to propagate through the interface towards the mid-span of the beam. There is significant scatter in interface slip measurements in duplicate specimens, and specimens did not behave consistently along the whole length of the specimen, due to the slip measurement depending on crack propagation and failure mode.

Zilch and Reinecke [52] stated that the load transfer mechanism of shear forces at a concrete to concrete interface, according to shear-friction theory, is composed of: a) adhesion; b) shear-friction; and c) shear reinforcement. According to the ASTM D907 [53] definition ‘‘adhesion is the state in which two surfaces are held together by interfacial forces which may consist of valence forces or interlocking action or both’’. When the ultimate load is reached, de-bonding take place at the interface and the shear stress will be transferred by mechanical interlocking. If the interface between two concrete layers is subject to compression stress, the shear stresses will be transferred by shear-friction. With a relative displacement increment between concrete layers, the reinforcement that crosses the interface will be put under tension and yielding can occur. Thus, the shear reinforcement will induce compression at the interface and the shear load will be transferred by friction. As slippage occurs, the shear reinforcement will be subjected to shear, termed dowel action [54]. There are several analytical models suggested by design codes for the calculation of shear strength at the concrete to concrete interface. The design codes of RC structures used to assess shear strength at the interface adopted in this study are Model Code (2010), Eurocode 2 [55], ACI Committee 318 [56], GRECO [51] code, and the CEB-FIP Model Code [57]. These design expressions are based on the shear-friction theory, as suggested by Birkeland and Birkeland [58], and the following four parameters are considered: a) normal stress at the interface; b) compressive strength of the weakest concrete; c) roughness of the substrate surface; and d) shear reinforcement crossing the interface [54].

The interface shear strength of the repaired/ strengthened RC beams can be obtained using the following Equations (1-4).

Model code 2010 [44], Eurocode 2 [55]:

$$\tau_{fud} = c \cdot f_{ctd} + \mu \cdot \sigma_N + \rho \cdot f_{yd} \cdot (\mu \cdot sin\alpha + cos\alpha) \leq 0.5 \cdot v \cdot f_{cd} \quad (1)$$

ACI Committee 318 [56] code:

$$\tau_{fud} = \lambda \cdot (1.79 + 0.6 \cdot \rho \cdot f_y \leq 3.45\ MPa \quad 3.45\ MPa \leq \tau_{fud} = \pi \cdot \rho \cdot f_{yd} \leq \min(0.2 \cdot f_{cd}, 5.5\ MPa \quad (2)$$

and $f_{yd} \leq 414\ MPa$

GRECO code [51]:

$$\tau_{fud} = \begin{cases} 0.25 \cdot f_{ct}, & smooth\ interface \\ 0.75 \cdot f_{ct}, & rough\ interface \\ f_{ct}, & use\ of\ shotcrete \end{cases} \quad (3)$$

CEB-FIP Model Code 1990 [57]:

$$\tau_{fud} = \begin{cases} 0.1 \cdot f_{ct}, & very\ smooth\ interface \\ 0.2 \cdot f_{ct}, & smooth\ interface \\ 0.4 \cdot f_{ct}, & rough\ interface \end{cases} \quad (4)$$

Where:

τ_{fud} is the design interface shear strength,

f_{ctd} is the design tensile strength of the concrete with the lower strength (between the old and the new concrete) and is given by $f_{ctd} = f_{ct}/\gamma_c$, where f_{ct} is concrete tensile strength estimated using compressive strength results and a formula proposed in the 2010 Model Code and γ_c = 1.5 for concrete,

f_y is steel yield stress, with design value of f_{yd},

σ_N is the external vertical to the interface stress,

α is the angle between reinforcement and interface level,

ρ is the geometric rate of interface reinforcement and λ is a modification factor reflecting the reduced mechanical properties of light- weight concrete relative to normal weight concrete and equals 1 for normal weight concrete.

c is the adhesion factor, and

μ is the friction factor which is affected by the interface type and representative values from Eurocode 2 [55] are presented in Table 8.

Table 8. Value of coefficients c and μ (Eurocode 2 [55]).

Type of Interface	c [MPa]	μ
Keyed	0.5	0.9
Rough	0.45	0.7
Smooth	0.35	0.6
Very smooth	0.25	0.5

The respective interface shear stress can be determined according to the British Standard BS 8110-1 [59] using Equation (5), and the respective results for each strengthened beam are presented in Table 9.

$$\tau_x = \frac{V_{sd}}{b \cdot z} \quad (5)$$

Where:

τ_x is the interface shear stress of the examined section of the beam according to BS 8110-1 (1997),

V_{sd} is the shear force of the examined section of the beam,

b is the width of the interface, and

z is the lever arm of the composite section.

The shear stress values for the maximum load (P_{max}) and for loads at 0.2 mm interface slip ($P_{s=0.2\ mm}$) have been calculated for all the examined specimens using Equation 5. These values together with the respective shear strength values calculated using the various available code provisions (Equations 1-4) for roughened interface are presented in Table 9.

Table 9. The interface shear strength and shear stress of the strengthened RC beams.

Specimen	Eurocode 2 [55] and Model Code 2010 [44] [MPa]	ACI-318 [56] [MPa]	GRECO [51] [MPa]	CEB-FIP Model Code 90 [57] [MPa]	τ_x (for P_{max}) [MPa]	τ_x (for $P_{(s=0.2\ mm)}$) [MPa]
NSC-S-1	0.91	1.79	1.51	0.81	2.67	1.50
NSC-S-2	0.91	1.79	1.51	0.81	2.80	1.52
NSC-S-corr-1	0.91	1.79	1.51	0.81	1.65	1.14
NSC-S-corr-2	0.91	1.79	1.51	0.81	1.78	0.92
PVAFRGC-S-1	0.91	1.79	1.51	0.81	2.73	1.45
PVAFRGC-S-2	0.91	1.79	1.51	0.81	2.62	1.69
PVAFRGC-S-corr-1	0.91	1.79	1.51	0.81	2.76	2.00
PVAFRGC-S-corr-2	0.91	1.79	1.51	0.81	2.84	1.98
SFRGC-S-1	0.91	1.79	1.51	0.81	2.91	2.20
SFRGC-S-2	0.91	1.79	1.51	0.81	3.02	1.96
SFRGC-S-corr-1	0.91	1.79	1.51	0.81	2.96	2.05
SFRGC-S-corr-2	0.91	1.79	1.51	0.81	2.79	1.30

Based on the values of Table 9, shear stress values at the maximum load (P_{max}) are higher than the shear strength values for all the examined cases. This is in agreement with the experimental observations which show interface slips especially in the specimens strengthened with NSC overlays. It needs to be mentioned at this stage that the examined models (Equations 1-4) are design models for conventional concrete –to-concrete interfaces and therefore it is expected that some of these models are quite conservative. However, it should be noted that the specimens with PVAFRGC and SFRGC which exhibited the highest

load capacities and therefore the highest shear strength values show very small interface slip values even if the maximum shear strength results of Table 9 are much higher than the relevant shear strength values of the code provisions. Therefore it can be concluded that the existing models are quite conservative in these cases.

By comparing the shear strength values of the various code provisions it is evident that ACI-318 [56] and GRECO [51] lead to shear strength values significantly higher than the respective values calculated using Eurocode 2 [55], Model Code 2010 [44], and CEB-FIP Model Code 90 [57]. The shear strength values calculated with Eurocode 2 [55], Model Code 2010 [44], and CEB-FIP Model Code 90 [57] are significantly lower than the respective shear stress values (τ_x) and therefore these can be considered quite conservative taking into account the fact that overall small interface slip values were observed and de-bonding was prevented (Fig. 24).

5. SUMMARY AND CONCLUSION

An experimental investigation was carried out on the performance of RC beams strengthened using a thin reinforced layer of NSC, PVAFRGC and SFRGC. The application of a PVAFRGC jacket on a RC beam was also investigated. The effect of severe environmental conditions on the flexural capacity of RC beams was evaluated by exposing RC beams to accelerated induced current. The results obtained can be summarized as follows:

- A PVAFRGC and SFRGC strengthening layer considerably reduced the effect of corrosion exposure on the mass loss of the reinforcement bar, crack distribution and flexural performance compared to the control RC beams and RC beams strengthened with NSC. Corroded NSC-S specimens showed a 37% reduction in load carrying capacity, while the corroded SFRGC specimens showed only a 3% reduction. There was no significant reduction in flexural performance of the corroded PVAFRGC specimens.
- The application of PVAFRGC for 3 side jacketing on a RC beam significantly improves the load bearing capacity. The ultimate load increased by 50% compared to the control RC beams.
- The application of a reinforced additional layer of NSC, PVAFRGC and SFRGC for the strengthening of RC beams is very effective, as the ultimate loading increase is about 2 times compared to control RC beams.
- Relatively small interface slip values were recorded in most of the examined specimens until the maximum load capacity of the strengthened beams and the effect of corrosion on the interface slip was negligible.
- Reduced interface slip values and therefore improved interface conditions were observed in the case of beams strengthened with reinforced PVAFRGC and SFRGC layers, compared to the respective results of specimens strengthened with reinforced NSC layers. The specimens with the Fibre Reinforced Geopolymer Layers (PVAFRGC and SFRGC) show relatively small values of interface slip (0.34-0.82 mm) which were acceptable for life safety levels (0.8 mm as specified by GRECO [50, 51]) even in the absence of any mechanical connectors.

- In the case of beams strengthened with PVAFRGC and SFRGC layers, de-bonding occurred at a late loading stage and after the maximum load capacity, due to shear crack propagation from the initial beam to the overlays.
- The strengthening technique using PVAFRGC and SFRGC materials provides a significant structural enhancement at the serviceability limit state resulting from a remarkable increase in the beam service load and stiffness, and increased durability, due to reduced crack widths and low permeability of the FRGC material.

Overall, the results of this study show that the application of FRGC is a promising novel technique for the enhancement of maximum load and ductility of existing RC elements, having at the same time improved durability characteristics. The technique is relatively simple, allowing curing of FRGC at ambient temperature, and the application shows sufficient connection with the initial RC beams just with the roughening of the surface of the existing element, without the need for mechanical connectors or adhesive at the interface. Future work should focus on the calculation of the actual interface properties and the adjustment of existing design models to take into account the improved characteristics of the FRGC-to-concrete interfaces.

ACKNOWLEDGEMENT

The lead author gratefully acknowledges the Iraqi Ministry of Higher Education and Scientific Research-University of Basrah and Iraqi Cultural Attaché in London for the award of a Doctoral Scholarship.

REFERENCES

[1] A. P. Lampropoulos, S. A. Paschalis, O. T. Tsioulou, and S. E. Dritsos, "Strengthening of reinforced concrete beams using ultra high performance fibre reinforced concrete (UHPFRC)," *Engineering Structures,* vol. 106, pp. 370-384, 1/1/ 2016.

[2] M. R. Maheri, S. Pourfallah, and R. Azarm, "Seismic retrofitting methods for the jack arch masonry slabs," *Engineering Structures,* vol. 36, pp. 49-60, 3// 2012.

[3] M. Di Ludovico, A. Prota, and G. Manfredi, "Structural upgrade using basalt fibers for concrete confinement," *Journal of composites for construction,* vol. 14, pp. 541-552, 2010.

[4] M. Kwon, H. Seo, and J. Kim, "Seismic performance of RC-column wrapped with Velcro," *Structural Engineering and Mechanics,* vol. 58, pp. 379-395, 2016.

[5] D. Anggawidjaja, T. Ueda, J. Dai, and H. Nakai, "Deformation capacity of RC piers wrapped by new fiber-reinforced polymer with large fracture strain," *Cement and Concrete Composites,* vol. 28, pp. 914-927, 2006.

[6] G. Martinola, A. Meda, G. A. Plizzari, and Z. Rinaldi, "Strengthening and repair of RC beams with fiber reinforced concrete," *Cement and Concrete Composites,* vol. 32, pp. 731-739, 10// 2010.

[7] S. M. Mourad and M. J. Shannag, "Repair and strengthening of reinforced concrete square columns using ferrocement jackets," *Cement and Concrete Composites,* vol. 34, pp. 288-294, 2// 2012.

[8] M. Grantham, C. Majorana, and V. Salomoni, "Introduction In: Proceedings of the international conference on concrete solutions," Italy: Padua., 2009.

[9] K. Kobayashi, T. Iizuka, H. Kurachi, and K. Rokugo, "Corrosion protection performance of High Performance Fiber Reinforced Cement Composites as a repair material," *Cement and Concrete Composites,* vol. 32, pp. 411-420, 2010.

[10] K. Kobayashi and K. Rokugo, "Mechanical performance of corroded RC member repaired by HPFRCC patching," *Construction and Building Materials,* vol. 39, pp. 139-147, 2013.

[11] N. Rajamane, M. Nataraja, N. Lakshmanan, and J. Dattatreya, "Rapid chloride permeability test on geopolymer and Portland cement," *Indian Concrete Journal,* pp. 21–6., 2011.

[12] S. Ahmad, "Techniques for inducing accelerated corrosion of steel in concrete," *The Arabian Journal for Science and Engineering,,* vol. 34, p. 95, 2009.

[13] CEB Bulletin d'Information 162, "Assessment of concrete structures and design procedures for upgrading (redesign)," ed. Losanne: CEB, 1983.

[14] H. Cheon and N. MacAlevey, "Experimental behaviour of jacketed reinforced concrete beams," *ASCE J Struct Eng,* vol. 126, pp. 692–9, 2000.

[15] D. A. Bournas and S. M. Raoof, "TRM versus FRP in flexural strengthening of RC beams: Behaviour at high temperatures, " Construction and building materials, vol. 154, pp. 424 437, 15/11/2017.

[16] N. H. Yi, J. W. Nam, S. B. Kim, I. S. Kim, and J.-H. J. Kim, "Evaluation of material and structural performances of developed Aqua-Advanced-FRP for retrofitting of underwater concrete structural members," *Construction and Building Materials,* vol. 24, pp. 566-576, 4// 2010.

[17] S.M. Raoof, L.N. Koutas, D.A. Bournas, "Textile-Reinforced Mortar (TRM)

versus Fibre-Reinforced Polymers (FRP) in flexural strengthening of RC beams, " Construction and building materials, vol. 151, pp. 279-291, 1/10/2017.

[18] N. Attari, S. Amziane, and M. Chemrouk, "Flexural strengthening of concrete beams using CFRP, GFRP and hybrid FRP sheets," *Construction and Building Materials,* vol. 37, pp. 746-757, 12// 2012.

[19] J.-h. Xie and R.-l. Hu, "Experimental study on rehabilitation of corrosion-damaged reinforced concrete beams with carbon fiber reinforced polymer," *Construction and Building Materials,* vol. 38, pp. 708-716, 2013.

[20] G. G. Triantafyllou, T. C. Rousakis, and A. I. Karabinis, "Corroded RC beams patch repaired and strengthened in flexure with fiber-reinforced polymer laminates," *Composites Part B: Engineering,* vol. 112, pp. 125-136, 2017.

[21] J. Cai, J. Pan, and X. Zhou, " Flexural behavior of basalt FRP reinforced ECC and concrete beams," *Construction and Building Materials,* vol. 142, pp. 423-430, 2017.

[22] F. U. A. Shaikh and A. Hosan, "Mechanical properties of steel fibre reinforced geopolymer concretes at elevated temperatures," *Construction and Building Materials,* vol. 114, pp. 15-28, 2016.

[23] K. Neocleous, H. Tlemat, K. Pilakoutas, "Design issues for concrete reinforced with steel fibres including fibres recovered from used tires," Journal of Materials in Civil Engineering ASCE, 18 (5), pp. 677-685, 1/10/2006.

[24] Z. Yunsheng, S. Wei, L. Zongjin, Z. Xiangming, Eddie, and C. Chungkong, "Impact properties of geopolymer based extrudates incorporated with fly ash and PVA short fiber," Construction and Building Materials, vol. 22, no. 3, pp. 370-383, 3//, 2008.

[25] M. H. Al-Majidi, A. Lampropoulos, and A. B. Cundy, "Tensile properties of a novel fibre reinforced geopolymer composite with enhanced strain hardening characteristics," *Composite Structures,* vol. 168, pp. 402-427, 5/15/ 2017.

[26] F.A. Farhat, D. Nicolaides, A. Kanelopoulos, B.L. Karihaloo, "High performance fibre-reinforced cementitious composite (CARDIFRC) – performance and application to retrofitting, " Engineering Fracture Mechanics, vol. 74(1–2), pp. 151-167, 1/1/2007.

[27] M. H. Al-Majidi, A. Lampropoulos, and A. B. Cundy, "Steel fibre reinforced geopolymer concrete (SFRGC) with improved microstructure and enhanced fibre-matrix interfacial properties," *Construction and Building Materials,* vol. 139, pp. 286-307, 5/15/ 2017.

[28] M. H. Al-Majidi, A. Lampropoulos, A. Cundy, and S. Meikle, "Development of geopolymer mortar under ambient temperature for in situ applications," *Construction and Building Materials,* vol. 120, pp. 198-211, 2016.

[29] L. Turner and F. Collins, "Carbon dioxide equivalent (CO2-e) emissions: A comparison between geopolymer and OPC cement concrete," *Construction and Building Materials,* vol. 43, pp. 125-130, 2013.

[30] C. Ouellet-Plamondon and G. Habert, "Life cycle analysis (LCA) of alkali-activated cements and concretes," *In Handbook of Alkali-Activated Cements, Mortars and Concretes*, WoodHead Publishing-Elsevier, Cambridge, pp. 663-686, 2015.

[31] J.L. Provis, A. Palomo, and C. Shi, "Advances in understanding alkali-activated materials," *Cement and Concrete Research*, vol. 78, pp. 110-125, 2015.

[32] S. Teh, T. Wiedmann, A. Castel, and J. de Burgh, "Hybrid life cycle assessment of greenhouse gas emissions from cement, concrete and geopolymer concrete in Australia, "*Journal of Cleaner Production*, vol. 152, pp. 312-320, 2017.

[33] F. Bencardino and A. Condello, "Eco-friendly external strengthening system for existing reinforced concrete beams," *Composites Part B: Engineering,* vol. 93, pp. 163-173, 2016.

[34] M. H. Al-Majidi, A. Lampropoulos, A. B. Cundy, O. Tsioulou and S. Alrekabi, " A novel corrosion resistant repair technique for existing reinforced concrete (RC) elements using polyvinyl alcohol fibre reinforced geopolymer concrete (PVAFRGC)," *Construction and Building Materials,* vol. 164, pp. 603-619, 2018.

[35] F. Pacheco-Torgal, Robert E. Melchers, Xianming Shi, Nele De Belie, Kim Van Tittelboom, Andrés Sáez (editors), "Eco-efficient Repair and Rehabilitation of Concrete Infrastructures," *Woodhead Publishing*, 2017.

[36] BS EN 450-1, "Fly ash for concrete. Definition, specifications and conformity criteria," ed: British Standards Institute, 2012.

[37] J. Davidovits, M. Izquierdo, X. Querol, D. Antennuci, H. Nugteren, V. Butselaar-Orthlieb, *et al.*, "The European Research Project GEOASH: Geopolymer Cement Based On European Coal Fly Ashes, Technical Paper #22," *Geopolymer Institute Library*, 2014.

[38] ASTM C490/C490M, "Standard Practice for Use of Apparatus for the Determination of Length Change of Hardened Cement Paste, Mortar, and Concrete.," ed. West Conshohocken, PA: ASTM International, 2011.

[39] S.-J. Lee and J.-P. Won, "Shrinkage characteristics of structural nano-synthetic fibre-reinforced cementitious composites," *Composite Structures,* vol. 157, pp. 236-243, 2016.

[40] F. G. Collins and J. G. Sanjayan, "Workability and mechanical properties of alkali activated slag concrete," *Cement and Concrete Research,* vol. 29, pp. 455-458, 1999.

[41] Z. Li, M. A. Perez Lara, and J. E. Bolander, "Restraining effects of fibers during non-uniform drying of cement composites," *Cement and Concrete Research,* vol. 36, pp. 1643-1652, 2006.

[42] C. Duran Atiş, C. Bilim, Ö. Çelik, and O. Karahan, "Influence of activator on the strength and drying shrinkage of alkali-activated slag mortar," *Construction and Building Materials,* vol. 23, pp. 548-555, 1// 2009.

[43] M. H. Al-Majidi, A. Lampropoulos, A. B. Cundy, O. Tsioulou and S. Alrekabi, "Fibre Reinforced Geopolymer versus Conventional Reinforced Concrete Layers for the structural strengthening of RC beams", IABSE Symposium, Nantes, France, 2018.

[44] fib Bulletin 55, "Model code 2010. Lausanne: International Federation for Structural Concrete (fib)," ed, 2010.

[45] J. E. Santos P, "Comparison of methods for texture assessment of concrete surfaces," *ACI Materials Journal*, vol. 107, pp. 433-440, 2010.

[46] ASTM E965-96, "Standard test method for measuring pavement macrotexture depth using a volumetric technique," in *American Society for Testing Materials*, 2006.

[47] ASTM G1-90(1999)e1, Standard Practice for Preparing, Cleaning, and Evaluating Corrosion Test Specimens, ASTM International, West Conshohocken, PA, 1999.

[48] M. Sahmaran, V. C. Li, and C. Andrade, "Corrosion resistance performance of steel-reinforced engineered cementitious composite beams," *ACI Materials Journal*, vol. 105, pp. 243-250, 2008.
[49] M. Sahmaran, O. Anil, M. Lachemi, G. Yildirim, A. F. Ashour, and F. Acar, "Effect of Corrosion on Shear Behavior of Reinforced Engineered Cementitious Composite Beams," *ACI Structural Journal*, vol. 112, 2015.
[50] O. T. Tsioulou, A. P. Lampropoulos, and S. E. Dritsos, "Experimental investigation of interface behaviour of RC beams strengthened with concrete layers," *Construction and Building Materials*, vol. 40, pp. 50-59, 2013.
[51] GRECO, "Greek retrofitting code (final version). Greek Organization for Seismic Planning and Protection. Athens: Greek Ministry for Environmental Planning and Public Works; 2012 [in Greek].", ed, 2012.
[52] K. Zilch and R. Reinecke, "Capacity of shear joints between high-strength precast elements and normal-strength cast-in-place decks," presented at the FIB International Symposium on High Performance Concrete, Orlando, USA, 2000.
[53] ASTM D907, "Standard terminology of adhesives," ed. West Conshohocken: ASTM International, 1996.
[54] P. M. D. d. Santos, "Assessment of the Shear Strength between Concrete Layers," PhD thesis, universidade de coimbra, 2009.
[55] Eurocode 2, "CEN En 1992–1-1, Design of concrete structures-Part 1–1: General rules and rules for buildings.," ed. Brussels:: European Committee for Standardization, 2004.
[56] ACI Committee 318, "Building code requirements for structural concrete (ACI318-99) and commentary (318R-99).", ed. Farmington Hills, MI:: American Concrete Institute, 1999.
[57]] CEB-FIP Model Code, "Model code for concrete structures," in *Comité Euro-International du Béton, Secretariat Permanent, Case Postale* vol. 88, ed. London: Thomas Telford, 1990.
[58] P. W. Birkeland and H. W. Birkeland, "Connections in precast concrete construction," in *Journal Proceedings*, 1966, pp. 345-368.
[59] BS 8110-1, "Structural use of concrete. Part 1: Code of practice for design and construction,," ed. London: British Standard Institute, 1997.